Submitted to the International Europhysics Conference on High Energy Physics,
HEP97, Jerusalem, Israel, August 1997

A Measurement of the Proton Structure Function $F_2(x, Q^2)$ at High Q^2 at HERA

H1 Collaboration

Abstract

New measurements of the proton structure function $F_2^p(x, Q^2)$ are reported. The results are obtained for momentum transfer squared Q^2 between 150 and 5000 GeV^2, and for Bjorken x values up to 0.32 using data collected by the HERA experiment H1 in 1995, 1996 and 1997 for a total integrated luminosity of about 22 pb^{-1}. This data sample has allowed an increase in precision compared with previous measurements. The data are compared to a Next-to-Leading Order QCD fit performed on the low Q^2 structure function data and found to be in good agreement with perturbative QCD.

Abstract 262
Parallel Sessions 3,4,7,313
Plenary Sessions PL 1,3,15,26

1 Introduction

Inclusive deep inelastic scattering (DIS) has already a long history of important discoveries attached to it, which helped for the understanding of the structure of matter and the establishment of the Standard Model. A large number of experiments done in the last three decades in the "fixed target" mode have constrained the parton densities in the proton, and stringently tested the predictions of Quantum Chromodynamics (QCD), the theory of the strong interaction which was developed following the first DIS results revealing the existence of partons in the proton [1]. At HERA, the first electron-proton collider ever built, the study of DIS has been further pursued since 1992 in new kinematic domains.

In the first years of operation the scattering at low momentum transfer squared Q^2 was explored, with particular attention to the region at low x, x being the fraction of the proton momentum carried by the struck parton. The measurements of the F_2 proton structure function revealed [2, 3] its strong rise with decreasing x and a behaviour which confirmed the predictions of perturbative Quantum ChromoDynamics (QCD) in the form of the Next-to-Leading Order (NLO) DGLAP [4] evolution equations. Further studies have been carried out recently at even lower x and Q^2 using, in 1995, the upgraded H1 and ZEUS detectors and a sample of events in which the event vertex was displaced in order to increase the angular acceptance of the scattered electron[1] [5, 6]. This study clearly showed the departure from the perturbative QCD regime, and opened a new field of investigation of the strong interaction.

A first glimpse in the higher Q^2 region was achieved with the 1994 data [7, 8] but the statistical precision of the data was insufficient to make stringent QCD tests. The data were shown to be in agreement with perturbative QCD up to 5000 GeV^2. Over the last 3 years of operation the integrated luminosity has grown by about an order of magnitude, rendering a new measurement possible at high Q^2 with an improved precision. The interest in the measurement is increased by the recent observation by H1 and ZEUS [9, 10] of a possible excess of events at Q^2 greater than about 15000 GeV^2 compared with Standard Model expectations.

From the cross-section measurement, the proton stucture function F_2 can be extracted, essentially without assumptions for the other structure functions F_L and xF_3 at Q^2 between 150 and about 2000 GeV^2. At higher Q^2 the contribution of xF_3 increases but reaches at most 15 % in the lowest x bin at $Q^2 = 5000$ GeV^2, and decreases rapidily with increasing x, such that F_2 can be safely extracted from the double-differential cross-section. The uncertainties due to F_L remain negligible in the high Q^2 range considered here since its influence on the cross-section is at most about 5% according to QCD calculations and was taken into account.

After a brief presentation of the H1 detector in section 2 and a reminder of the kinematic reconstruction in section 3, the simulation programs which have been used to extract F_2 are presented in section 4. The event selection and the calibration procedures are discussed in section 5. The measurement of the cross-section and the extraction of the F_2 structure function are presented in section 6. A summary is given in section 7.

2 The H1 Detector

The H1 detector [11] is a nearly hermetic multi-purpose apparatus built to investigate the deep inelastic scattering of electrons and protons at HERA. The high Q^2 structure function measurement relies primarily on the tracking chamber system, on the liquid argon (LAr) calorimeter,

[1] At HERA, since 1994, the collisions involve protons and positrons. In this paper, we use the word "electron" both for electron and positron.

on the luminosity detectors, and on a lesser extent on the backward calorimeter[2]. They will be described briefly in the following.

The tracking system includes the central tracking chambers and the forward tracker modules. These chambers are placed around the beampipe at z positions between -1.5 and 2.5 m. A superconducting solenoid surrounding both the tracking system and the (LAr) calorimeter provides a uniform magnetic field of 1.15 T.

The central jet chamber (CJC) consists of two concentric drift chambers covering a polar angular range from 15^o to 165^o. All polar angles are defined with respect to the proton direction. Tracks crossing the CJC are measured with a transverse momentum resolution of $\delta p_T/p_T < 0.01 \cdot p_T/\mathrm{GeV}$. The CJC is supplemented by two cylindrical drift chambers at radii of 18 and 47 cm, respectively, to improve the determination of the z coordinate of the tracks. A tracking chamber system made of three identical modules measures hadrons emitted in the forward direction (7^o to 20^o). The forward tracker is used to determine the event vertex for the events which leave no track in the CJC.

The scattered electron and most of the hadronic final state energy are measured in the LAr calorimeter [12] which covers an angular region between 3^o and 155^o. The calorimeter consists of an electromagnetic section with lead absorber plates and a hadronic section with stainless steel absorber plates. Both sections are highly segmented in the transverse and longitudinal directions with about 44000 cells in total. The electromagnetic part has a depth between 20 and 30 radiation lengths. The total depth of both calorimeters varies between 4.5 and 8 interaction lengths (λ_I). The electromagnetic energy uncertainty of the LAr calorimeter is determined to be less than 3%, obtained by a study of the "kinematic peak" of the electron energy spectrum at medium Q^2 ($100 < Q^2 < 1000$ GeV^2), and complemented at higher Q^2 by studies using further kinematic constraints. The hadronic energy uncertainty of the LAr calorimeter is determined to be 4% by cross-calibration *in situ* with the low Q^2 scattered positron. This is confirmed at high Q^2 but with a lower statistical precision. The LAr calorimeter is also used for the triggering of high Q^2 events, by means of the detection of a "tower" of electromagnetic energy [11] deposited by the scattered electron. Above the threshold energy of the analysis, 11 GeV, the trigger efficiency is greater than $99 \pm 1\%$.

In the backward region, a lead/scintillating fiber calorimeter (SPACAL) [13] was installed in 1995 to replace the previous lead/scintillator electromagnetic calorimeter (BEMC). The new calorimeter has both an electromagnetic and hadronic section with a total depth of about 2 λ_I. Its angular acceptance ($153^o < \theta < 177.8^o$) allows, in conjunction with the LAr calorimeter, for a quasi-complete containment of the hadronic final state. The hadronic energy scale uncertainty of the measurement in the SPACAL is presently about 7%. However its influence on the high Q^2 events is very small.

The luminosity was determined from the measured cross section of the Bethe Heitler (BH) reaction $ep \to ep\gamma$. The final state electron and photon can be detected in calorimeters (electron and photon "taggers") close to the beampipe at large distances from the main detector (at $z = -33$ m and $z = -103$ m). For the final value of the luminosity only the hard photon bremsstrahlung data were used. The precision of the luminosity determination is 2% [14].

3 Kinematics

The kinematic variables of the inclusive scattering process $ep \to eX$ can be reconstructed in different ways using measured quantities from the hadronic final state and from the scattered

[2]The positive z axis is defined at HERA as the incident proton beam direction.

electron. The choice of the reconstruction method for Q^2 and y determines the size of systematic errors, acceptance and radiative corrections.

The methods used in this measurement are: i) the so called "electron method" (E), using apart from the event vertex only the information of the scattered electron, which has the best resolutions in x and Q^2 at large y; ii) the so called "Σ method" [15] (Σ), calculated from the electron and hadronic final states measurements, which has small radiative corrections and extends from very low to large y values. Both calorimetric and track information are used to calculate the kinematics with the Σ method.

The application of different methods allows for a better understanding of the measurement and its systematic errors. In general x is obtained from Q^2 and y via $x = Q^2/ys$, so in the following we just remind the y and Q^2 formulae. The basic methods are the E and Σ methods:

$$y_e = 1 - \frac{E'_e}{E_e}\sin^2\frac{\theta_e}{2} \qquad\qquad Q^2_e = \frac{E'^2_e \sin^2\theta_e}{1-y_e} \tag{1}$$

where E'_e and θ_e are the energy and polar angle of the scattered electron. For the study of the hadronic final state, it is convenient to introduce the quantity Σ, the total transverse momentum $p_{T,h}$ and the inclusive hadronic angle γ defined by:

$$\Sigma = \sum_h (E_h - P_{z,h}). \qquad p_{T,h} = \sqrt{(\sum_h p_{x,h})^2 + (\sum_h p_{y,h})^2} \qquad \tan\frac{\gamma}{2} = \frac{\Sigma}{p_{T,h}} \tag{2}$$

Here E_h and $P_{z,h}$ are the energy and longitudinal momentum component of a particle h, the summation is over all hadronic final state particles and the masses are neglected. The formulae for the Σ method are then given by:

$$y_\Sigma = \frac{\Sigma}{\Sigma + E'_e(1-\cos\theta_e)} \qquad\qquad Q^2_\Sigma = \frac{E'^2_e \sin^2\theta_e}{1-y_\Sigma} \tag{3}$$

The kinematics can also be reconstructed using the double-angle (DA) [16] method in which y and Q^2 are derived from θ_e and γ. The DA method has been used to cross-check successfully the measurement presented in this paper. At high Q^2 the differences between the methods tend to diminish, since, with increasing Q^2, the DA method improves, the hadronic final state is measured in a better way, and the low y region, in which the E method is poor, slowly becomes kinematically inaccessible.

4 Monte Carlo Programs

Acceptance corrections and background contributions are studied with the data and Monte Carlo programs. Monte Carlo DIS events corresponding to between 3 (60) times the luminosity of the data at medium (very high) Q^2, were generated using DJANGO [17]. This program is based on HERACLES [18] for the electroweak interaction and on LEPTO [19] to simulate the hadronic final state. HERACLES includes complete first order radiative corrections, and the simulation of real bremsstrahlung photons. LEPTO uses the colour dipole model (CDM) as implemented in ARIADNE [20] which is in good agreement with data on the energy flow and other characteristics of the final state as measured by H1 [21] and ZEUS [22]. The hadronization is performed using string fragmentation [23]. The acceptance corrections were performed after "reweighting" the simulation, produced with the MRSH [24] parton distributions, to the H1 QCD fit [25], but performed only on the H1 low Q^2 data (1994-1996), and on the BCDMS and NMC data. The two fits give essentially the same result.

The photoproduction background was simulated using the PYTHIA [26] generator for γp interactions. A sample of photoproduction events of the "direct" ("resolved") type of 2.5 (5) times the data luminosity was generated and, after a preselection for being potential background events, the events were simulated in the detector. The potential background originating from prompt photon production was studied on a simulated sample [27] representing 30 times the luminosity of the data.

Based on the GEANT program [28] the detector response was simulated in detail. After this step the Monte Carlo events were subject to the same reconstruction and analysis chain as the real data.

5 Event Selection and Calibration

The data sample used for the measurements at $Q^2 \leq 5000$ GeV^2 corresponds to an integrated luminosity of about 22 pb^{-1}. The events obtained by the LAr calorimeter based trigger, were preselected by asking that:

- the most energetic calorimeter cluster in the event has an energy greater than 11 GeV;
- an event vertex is reconstructed from the central or forward tracker within 35 cm of the average event vertex position;
- the $E - p_z$ ($\equiv \Sigma + E'_e(1 - \cos\theta_e)$) of the event is greater than 35 GeV and smaller than 75 GeV, when using the. For a perfectly reconstructed event this quantity is equal to 55 GeV, i.e. two times the electron beam energy. This requirement reduces the background and the radiative corrections.

The events were studied in two independent analyses, using two different electron identification, two reconstruction methods and two sets of kinematic cuts. The results have been found to be independent of the details of these analyses.

The electron identification relies mainly on two requirements

- the electromagnetic cluster must be compact, i.e. at least 70% of the energy is contained in the 4 most energetic cells of the cluster.
- there is a charged track, the extrapolated trajectory of which, has a distance of closest approach (DCA) to the center of gravity of the cluster of less than 12 cm. The track is used for the (θ_e) determination. At $\theta < 40°$ this condition is not enforced, and the angle is determined from the cluster if there is no track pointing to the cluster. In that case the $E - p_z$ requirement is set to 35 GeV for the E method also.

The selection cuts were designed to have a high efficiency for detecting DIS events. For a large part of the kinematic region studied the total efficiency is better than 80%.

At high Q^2 the main sources of non-ep background to DIS events are due to cosmic rays, and so-called "halo"-muons, which are parallel to the beam and can induce electromagnetic showers. They are both effectively reduced by the previous cuts, and rejected by dedicated filters. The requirement that the event time which is accurately determined in the CJC coincides with the nominal time of the bunch crossing of the beams, finally render these backgrounds completely negligible.

The physical background to DIS from ep interactions is due to photoproduction events at $Q^2 \simeq 0$ where the scattered electron escapes the detector along the beampipe but in which an energy cluster from the hadronic final state fakes an electron. The total photoproduction background was estimated from studies using simulated events from the Monte Carlo program PYTHIA, and checked using the fraction of data events which are "tagged" in a dedicated electron detector located close to the beam pipe. These events accumulate at high y, and a kinematic cut at $y_e < 0.9$ of the assumed electron candidate greatly reduces it. The remaining photoproduction background was subtracted statistically bin by bin using this prediction. For each Q^2 value, only the smallest x bin can have contamination larger than 3%. This contamination never exceeds 10% in any bin. Other backgrounds [9] are all significantly smaller than that due to photoproduction.

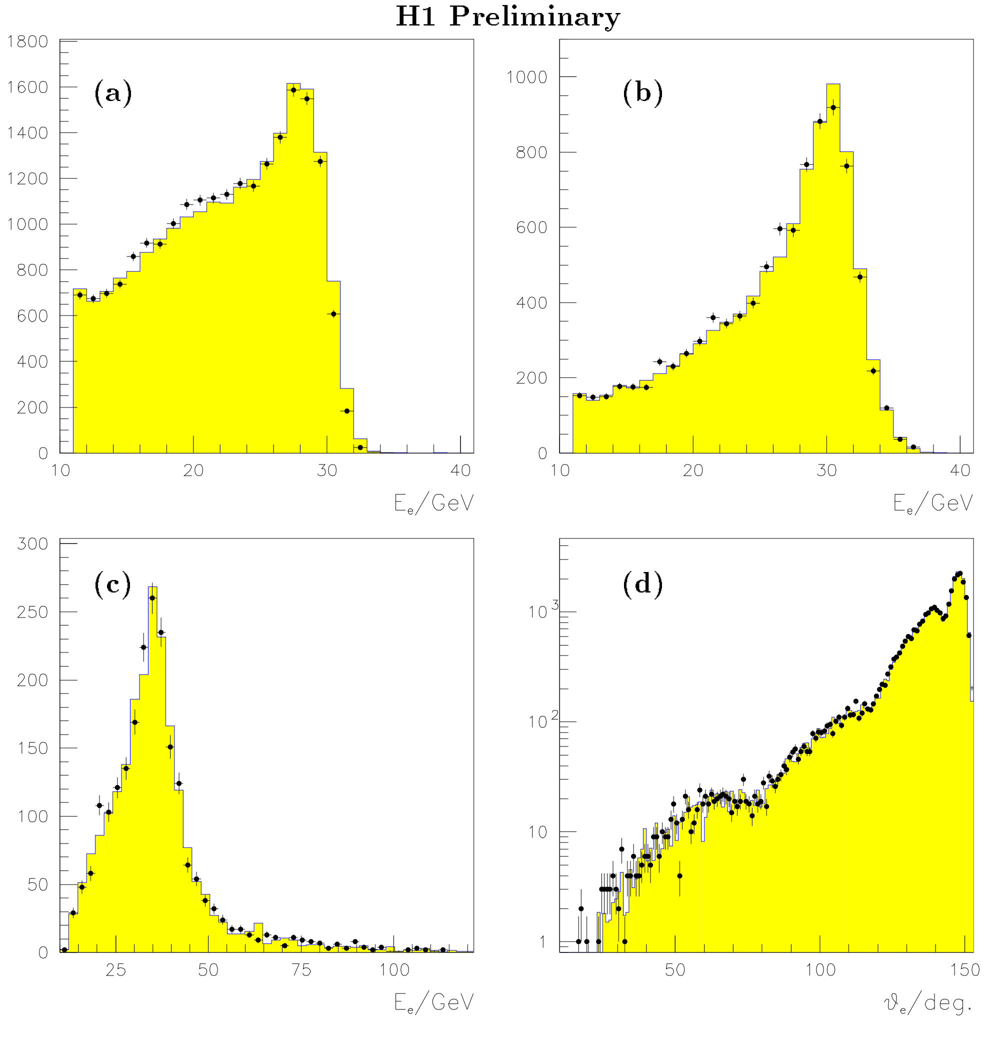

Figure 1: *Energy spectrum of the scattered electron at Q^2 between 150 and 350 GeV^2 (a), between 350 and 1000 GeV^2 (b), and greater than 1000 GeV^2 (c). Polar angle spectrum of the scattered electron (d). The simulation (histogram) normalized to luminosity is compared to the data (points).*

The response of the detector has been studied in detail using the almost complete containments of these events, and the overconstrained kinematics. For instance the energy of the electron can be predicted within 1% precision from the values of θ_e and γ at y below 0.1. Regions, both in z and in ϕ, in which the dead materials was found to spoil the response of the electron by more than about 5% were cut from the analysis, both in the data and in the simulated sample.

Overall, about 20% of the events were removed in this way.

The energy spectrum of the remaining events are given in fig. 1a,b,c for 3 different Q^2 intervals ($150-350$, $350-1000$, >1000 GeV^2). The description of the data by the simulation confirms the understanding of the energy scale, which is controlled to within 3% in the whole detector. The θ_e distribution in fig. 1d is distorted due to the fiducial cuts. The good agreement between the data and the simulation shows that these cuts are well understood.

The hadronic final state calibration is checked with the electron both at low and high Q^2. The distribution of the ratio of the y values measured with the Σ and E method y_Σ/y_e at high Q^2 is shown in fig. 2a, for $y_e > 0.05$. This distribution is a good test of the hadronic response in the central/backward part of the detector, since the contribution of the forward hadronic energy to the y_Σ is by construction small. In fig. 2b, the transverse momentum of the hadronic system divided by the scattered electron, $p_{T,h}/p_{T,e}$, is shown. In both distributions the agreement between the electron and the hadronic final state variables is satisfactory, and the simulation reproduces the experimental distributions.

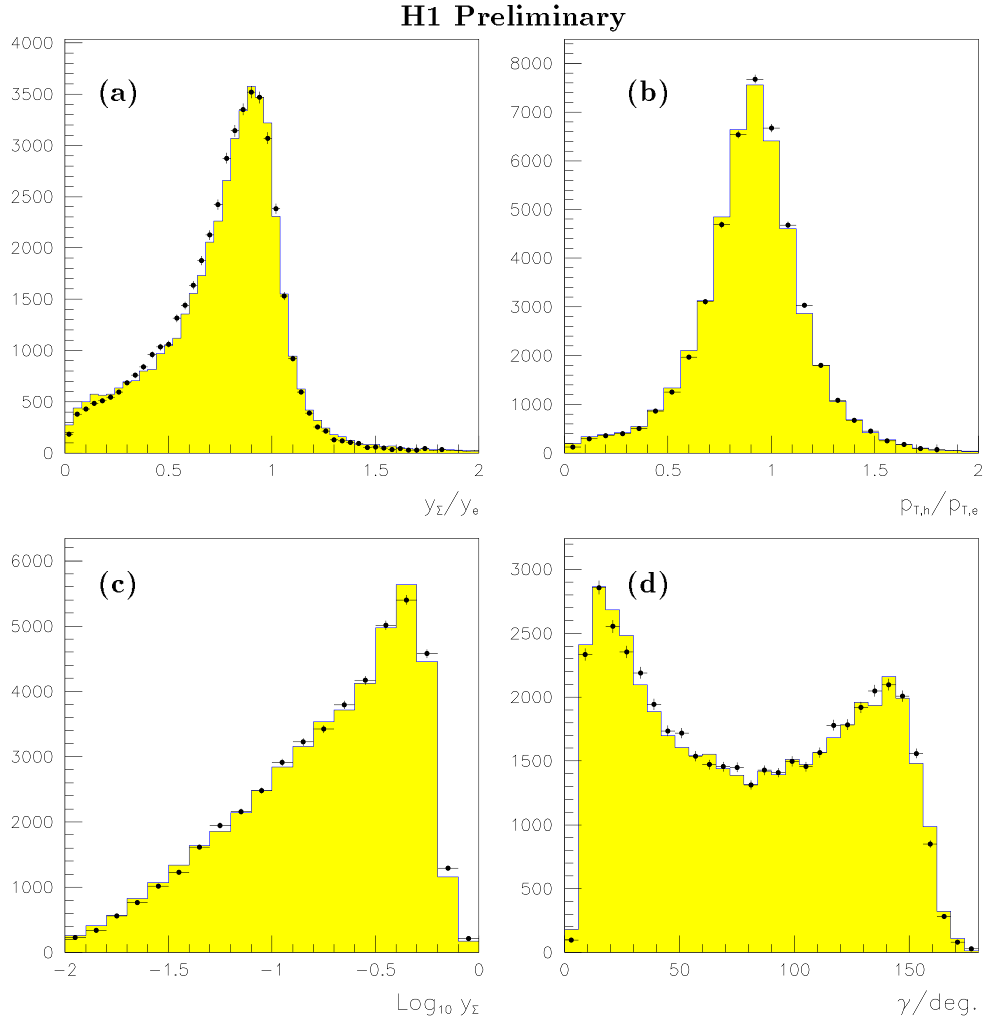

Figure 2: *Ratio of y_Σ/y_e (a) at $y_e > 0.05$; ratio of $p_{T,h}/p_{T,e}$ (b); Distribution of $Log_{10}(y_\Sigma)$ (c); Distribution of the hadronic angle (d). The simulation (histogram) normalized to luminosity is compared to the data (points).*

The quality of the measurement can also be judged in fig. 2c in which the y_Σ distribution is compared to the simulated one or in fig. 2d which shows the distribution of the hadronic angle

γ. The agreement extends from the lowest (0.01) to the highest (0.9) accessible y, and from the lower to the higher angles. All these studies demonstrate that the quoted uncertainty of 4% on the hadronic energy response is appropriate.

6 Cross-Section and Structure Function Measurements

The inclusive cross section for the NC DIS reaction $e^+ + p \to e^+ + X$ with unpolarized beams is

$$\frac{\mathrm{d}^2\sigma}{\mathrm{d}x\ \mathrm{d}Q^2} = \frac{2\pi\alpha^2}{xQ^4}\left[Y_+ F_2(x,Q^2) - y^2 F_L(x,Q^2) - Y_- xF_3(x,Q^2)\right](1+\delta_r(x,Q^2)) \qquad (4)$$

In this equation α is the fine structure constant, F_2 is the generalized structure function which contains both photon and Z° exchange, F_L is the longitudinal structure function, F_3 contains the parity violating term arising from the Z° exchange, and δ_r is the electroweak radiative correction, allowing to extract the Born cross-section from the measured one. The helicity dependence of electroweak interactions, is contained in the functions

$$Y_\pm = 1 \pm (1-y)^2. \qquad (5)$$

According to QCD calculations the contribution of F_L is small in the high Q^2 region, below 5% at the highest $y = 0.9$ of this analysis, and negligible at lower y. The radiative corrections are made using the HERACLES program.

The generalized F_2 structure function can be written as

$$F_2 = F_2^{em} + \frac{Q^2}{(Q^2+M_Z^2)} F_2^{int} + \frac{Q^4}{(Q^2+M_Z^2)^2} F_2^{wk} = F_2^{em}(1+\delta_Z) \qquad (6)$$

where M_Z is the mass of the Z° and F_2^{em} , F_2^{wk} and F_2^{int} are the contributions to F_2 due to photon exchange, Z° exchange and γZ° interference respectively.

In the kinematic range investigated the effect of the $\gamma - Z$ interference is still small, so that it is possible to extract from the measured differential cross section F_2^{em} (i.e. F_2 corresponding to QED). The difference between F_2 and F_2^{em} in the Standard Model is expected to be less than 1% for values of $Q^2 < 1000$ GeV^2. In the region of high Q^2, the xF_3 term reduces slightly the e^+p cross section. The largest correction from the combined F_2^{int}, $F_2^{wk}$and xF_3 contributions is about 10% in the lowest x bin at $Q^2 = 5000$ GeV^2, but is lower than 1% for $Q^2 < 1500$ GeV^2.

In summary, in this analysis we measure the double-differential cross-section at Q^2 between 150 and 5000 GeV^2 and we extract from this measurement the structure function F_2^{em} up to $Q^2 = 5000$ GeV^2. So, as in the previous H1 structure function publications, we define in the following as $F_2 \equiv F_2^{em}$.

A general procedure to determine F_2 is described in [7]. The data were binned in a $Q^2 - x$ grid, with 8 (5) bins per order of magnitude in Q^2 (x), except at $Q^2 > 2000$ GeV^2, for which a coarser bin in Q^2 was adopted to compensate for the rapidly decreasing number of events. The number of events reconstructed in a bin which originates from that bin is larger than 40% for the E method and larger than 30% for the Σ method. All detector efficiencies were determined from the data using the redundancy of the apparatus. They are correctly reproduced by the Monte Carlo simulation within the small errors quoted below, and therefore the Monte Carlo could be used to correct for the detector acceptance. The list of systematic errors considered is:

- A potential miscalibration of the electron energy of 3%.
- A 4% scale error for the hadronic energy in the LAr calorimeter. A 7% scale error was assigned to the energy of the hadronic final state measured in the SPACAL.
- A potential shift of up to 3 mrad for the electron polar angle.
- A potential error on the radiative corrections: 2%.

- The following contributions to the systematic errors from the event selection were included:
  - A conservative error on the electron identification efficiency of 3%.
  - vertex finding efficiency: 2%.
  - The uncertainty due to photoproduction background was assumed to be 50% of the correction applied, i.e. smaller than 5%. This affects only the highest y bins.

These systematic uncertainties affect differently the F_2 measurement made with different methods. In Fig. 3 the comparison of the measurement made with the E and with the Σ method is shown, with the statistical and systematic errors added in quadrature. The good agreement between the two measurements indicates that the errors are correctly estimated.

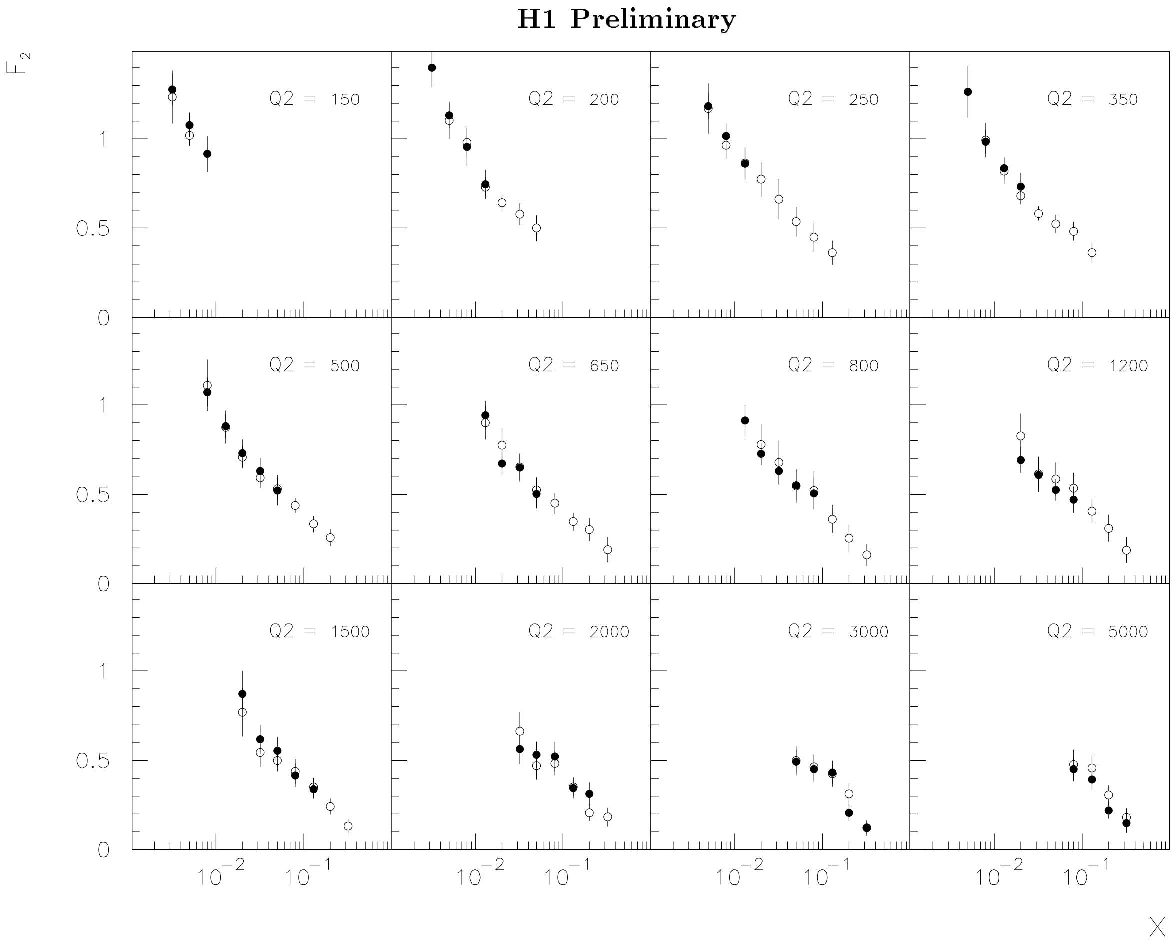

Figure 3: *Comparison of F_2 measurements using the E method (black points) and the Σ method (open points). The error bars represent the quadratic sum of the statistical and systematic error.*

The final results are then taken to be those using the E method at $y > 0.15$ and the Σ method at $y < 0.15$. The result is shown in fig. 4 and compared to the H1 QCD fit [25] which does not use data at $Q^2 > 120$ GeV^2. The agreement is good up to the highest Q^2 showing that the perturbative QCD expectations based on NLO DGLAP evolution is able to describe the measurements up to 5000 GeV^2.

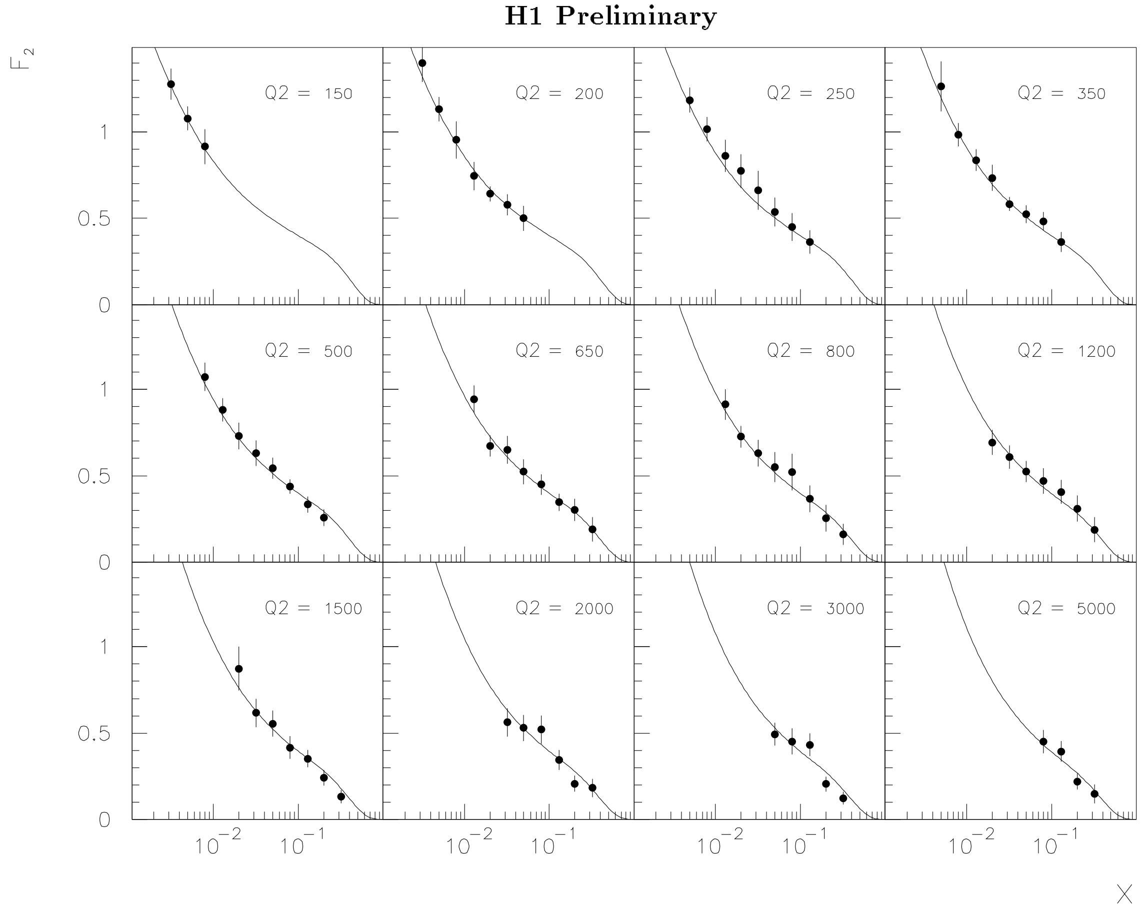

Figure 4: *Preliminary H1 measurement of F_2 at high Q^2. The error bars represent the quadratic sum of the statistical and systematic error. The curve represent a NLO QCD fit to the H1 1994, 1995 and 1996 low Q^2 ($\leq$ 120 GeV^2) data, together with the NMC and BCDMS data. The data are in good agreement with the fit.*

7 Summary

A precise measurement of the proton structure function has been performed at high Q^2 with the H1 detector, using the data collected from 1995 to 1997. The double differential cross-section $\mathrm{d}^2\sigma/\mathrm{d}x\mathrm{d}Q^2$ has been measured from 150 to 5000 GeV^2, from which the proton structure function $F_2(x, Q^2)$ has been extracted with a precision of about 10% below 1000 GeV^2, and about 18% at 5000 GeV^2. The prediction of perturbative QCD in the form of the NLO DGLAP evolution compared with the measurements of F_2 for $Q^2 \leq 120$ GeV^2 is able to decribe these new measurements in the range of 150 GeV^2 $\leq$Q^2 $\leq$ 5000 GeV^2.

1

Acknowledgements

We are grateful to the HERA machine group whose outstanding efforts have made and continue to make this experiment possible. We thank the engineers and technicians for their work in constructing and now maintaining the H1 detector, our funding agencies for financial support, the DESY technical staff for continual assistance, and the DESY directorate for the hospitality which they extend to the non-DESY members of the collaboration.

References

[1] E.D. Bloom, F.J. Gilman, Phys.Rev.Lett. **22** (1969) 1.

[2] H1 Collab., I. Abt et al., Nucl. Phys. **B407** (1993) 515.
H1 Collab., T. Ahmed et al., Nucl. Phys. **B439** (1995) 471.

[3] ZEUS Collab., M. Derrick et al., Phys. Lett. **B316** (1993) 412.
ZEUS Collab., M. Derrick et al., Z. Phys. **C65** (1995), 379.

[4] Yu. L. Dokshitzer, Sov. Phys. JETP **46** (1977) 641;
V. N. Gribov and L.N. Lipatov, Sov. J. Nucl. Phys. **15** (1972) 438 and 675;
G. Altarelli and G. Parisi, Nucl. Phys. **B126** (1977) 297.

[5] H1 Collab., C. Adloff et al., DESY preprint 97-042 (1997)

[6] ZEUS Collab., J. Breitweg et al., DESY preprint 97-135 (1997).

[7] H1 Collab., S. Aid et al., Nucl. Phys. **B470** (1996) 3.

[8] ZEUS Collab., M. Derrick et al., Z. Phys. **C72** (1996) 399.

[9] H1 Collab., C. Adloff et al., Z. Phys **C74** (1997) 191.

[10] ZEUS Collab., J. Breitweg et al., Z. Phys. **C74** (1997) 207.

[11] H1 Collaboration, I. Abt et. al., Nucl. Instr. and Meth. **A386** (1997) 310 and 348.

[12] H1 Calorimeter Group, B. Andrieu et al., Nucl. Instr. and Meth. **A336** (1993) 460.

[13] R.D. Appuhn et al., Nucl. Instr. and Meth. **A386** (1997) 397.

[14] H1 Collab., Luminosity Measurement in the H1 Experiment at HERA (submitted to ICHEP96: pa17-026).

[15] U.Bassler, G.Bernardi, Nucl. Instr. and Meth. A361 (1995) 197.

[16] S.Bentvelsen et al., Proceedings of the Workshop Physics at HERA, vol. 1, eds. W.Buchmüller, G.Ingelman, DESY (1992) 23-40.
C.Hoeger, ibid., 43-55.

[17] G. A. Schuler and H. Spiesberger, Proceedings of the Workshop Physics at HERA, vol. 3, eds. W. Buchmüller, G. Ingelman, DESY (1992) 1419.

[18] A. Kwiatkowski, H. Spiesberger and H.-J. Möhring, Comp. Phys. Comm. **69** (1992) 155.

[19] G. Ingelman, Proceedings of the Workshop Physics at HERA, vol. 3, eds. W. Buchmüller, G. Ingelman, DESY (1992) 1366.

[20] L. Lönnblad, Computer Phys. Comm. **71** (1992) 15.

[21] H1 Collab., I. Abt et al., Z. Phys. **C63** (1994) 377.

[22] ZEUS Collab., M. Derrick et al., Z. Phys. **C59** (1993) 231.

[23] T.Sjöstrand and M.Bengtsson, Comp. Phys. Commun. **43** (1987) 367;
H.-U.Bengtsson and T.Sjöstrand, Comp. Phys. Commun. **46** (1987) 43;
T.Sjöstrand, CERN-TH-6488 (1992).

[24] A.D Martin, W.J. Stirling and R.G. Roberts, Phys. Lett. **B306** (1993) 145; **B309** (1993).

[25] H1 Collaboration, A Measurement of the Inclusive Deep Inelastic ep Scattering Cross Section at low Q^2 at HERA, submitted to IECHEP 97 (1997).

[26] PYTHIA, T. Sjöstrand, CERN-TH.7112/93 (1993)

[27] T.Sjöstrand, CERN-TH-6488 (1992) Comp. Phys. Comm. **82** (1994) 74.

[28] R. Brun et al., GEANT3 User's Guide, CERN–DD/EE 84–1, Geneva (1987).